Journal of Intelligent & Robotic Systems (2021) 102:75
https://doi.org/10.1007/s10846-020-01266-1

REGULAR PAPER

A Climbing Robot for Steel Bridge Inspection

Son Thanh Nguyen[1] · Hung Manh La[2]

Received: 8 January 2020 / Accepted: 2 October 2020

Abstract

As an effort of automating the bridge inspection process, this paper presents a new development of an adaptable tank-like robot, which can climb on steel structures to collect data and perform inspection. While most current steel climbing mobile robots are designed to work on flat steel surface, our proposed tank-like robot design is capable of climbing on different steel structural shapes (e.g., cylinder, cube) by using reciprocating mechanism and magnetic roller-chains. The developed robot can pass through the joints and transition from one surface to the other (e.g., from flat to curving surfaces). A prototype robot integrating multiple sensors (hall-effects, IR, IMU, Eddy current and cameras), has been developed by coping with variety of strict concerns including tight dimension, effective adhesive and climbing adaptation. Rigorous analysis of robot kinematics, adhesive force, sliding and turn-over failure and motor power has been conducted to certify the stability of the proposed design. The theory calculations can serve as an useful framework for designing future steel climbing robots. The cameras and Eddy current sensor is integrated on Robot for visual and in-depth fatigue crack inspection of steel structures. Experimental results and field deployments on more than twenty steel bridges confirm the adhesive, climbing, inspection capability of the robot. Video of this deployment can be seen in this link: https://youtu.be/1Wl9Trd3EoM.

Keywords Field robotics · Climbing robots · Magnetic wheel robots · Steel bridge inspection · Structure health monitoring

1 Introduction

1.1 Motivation

Bridges in general and steel bridges in particular are vital parts of transport infrastructure. There are more than 607,380 bridges in the United States [1]. Of this total, 200,000 bridges are steel, and about 25% of these steel bridges are either deficient or functionally obsolete, indicating a growing threat to the safety of transportation. The collapse of several bridges recently (e.g., I-5 Skagit River Bridge collapse [2] in Washington State in May 2013) has shown significant impact on the safety of travelers. Therefore, the bridges require more frequently inspection in order to timely monitor their structural health. However, the current inspection practice is mainly by visual (see Fig. 1) and manual nondestructive testing/evaluation and hence can not meet the demand for frequent and adequate inspection and maintenance [1, 3].

The inspection on steel bridges often takes place at height, limited/confined space and dangerous environments or at inaccessible areas sometime (see Fig. 1). These works demand skillful inspectors, and it is time consuming and also costly for training and operation. There is a significant motivation for automating the bridge inspection and evaluation through the development of climbing robots, which can seamlessly support the inspectors to complete their jobs in an efficient manner. Thus, the automated inspection is an expected solution, in which robot is able to climb on steel bridges, carry cameras and nondestructive evaluation (NDE) sensors to collect data and update infrastructure's health. However, design and development of a such climbing robot is challenging because it requires that the robot is able to climb, adhere (without falling off) and transition on complex steel structures with various shapes. In addition, the robot should be able to perform data collection in the confined space. This paper presents a new design and development of a climbing robot to

✉ Hung Manh La
hla@unr.edu

Son Thanh Nguyen
thanhson@nevada.unr.edu

[1] Advanced Robotics and Automation (ARA) Lab, University of Nevada, 1664 N. Virginia Street, Reno, NV 89557, USA

[2] ARA Lab, University of Nevada, 1664 N. Virginia Street, Reno, NV 89557, USA

Published online: 05 July 2021

Fig. 1 Current practice of steel bridge inspection: rope certified bridge engineers inspecting the Golden Gate bridge, San Francisco, California , source: NBC April 2018. Detail available here: https://www.nbcbayarea.com/on-air/as-seen-on/Inspections-Continue-at-Golden-Gate-Bridge_Bay-Area-312301361.html

tackle these challenges. The difficult maneuverability on complex steel structures is overcome through an integrated design of reciprocating mechanism and permanent magnetic roller-chains. The NDE data collection is eased by the development and integration of two 5 degree-of-freedom (DOF) robotic arms (one on the robot and one on the operator's hand) to allow the operator/user to observe and manage data collection.

1.2 Literature Review

As an effort to automate the inspection process, there has been variety of implementations of climbing robots for inspection [4–8]. A notable development of steel climbing robots is summarized in Fig. 2. A roller chain, integrated permanent magnets robot was reported in [9]. A legged robot that can transition across structure members for steel bridge inspection was developed [10]. The robot uses permanent magnets integrated with each foot to allow it to hang from a steel bar. In another case, a magnetic wheeled robot, which can carry magneto resistive sensor array for detecting corrosion and cracks, was developed [11]. Similarly, several climbing permanent magnet-robots [12–20] were designed to carry non-destructive evaluation (NDE) devices to detect corrosion, weld defects and cracks, and these robots can be applied for inspecting steel structures and bridges. Other efforts have shown for development of climbing robots for power plant inspection [21] and bridge cable inspection [22]. Additionally, significant development of climbing robots for steel structure and bridge inspection has been reported in [4, 23–33]. Furthermore, with industry involvement, a surface adapting tank-like robot with untouched permanent magnet mechanism was developed by Inuktun company for steel structure inspection using camera for visual observation [34].

In addition to using permanent magnet, electromagnet was also used to develop a climbing robot. For instance, electromagnet was embedded on a spider robot's legs [35] to utilize the climbing ability of the creature on complex structures.

Apart from steel bridge inspection, the great effort for automating concrete bridge deck inspection and evaluation has been reported in [36–46]. The leading work in the automated concrete bridge deck inspection is the Robotics Assisted Bridge Inspection Tool (RABIT^{TM}), which was developed by the the Rutgers University's Center for Advanced Infrastructure and Transportation. RABIT was integrated with multiple NDE sensors including ground penetrating radar, electrical resistivity, impact echo, ultra surface wave and high resolution cameras [37]. RABIT can move autonomously on bridge deck to collect visual and NDE data by using the Extended Kalman Filter (EKF)-based localization and the artificial potential field-based motion planning [40, 47].

Last, but not least, drones are also contributed in this area. In [48], the author introduced the multicopter carrying high resolution camera for bridge inspection tasks. The remote building inspection and monitoring by drone application mentioned in [49]. The deeper researches for energy optimization and visual data quality was reported in [50–52]. Recently, Intel Corp. also involved with the drone development for bridge inspection [53].

In summary, most existing designs are developed for particular application with limited functions. Some provide visual inspection only, and some use untouched magnets,

Robot	Type of Locomotion	Detail	Climbing Ability	Adhesion Method
Mecanum-wheel Robot [Kamdar2015] 	4-mecanum wheels	681 × 559 × 323 mm 34 kg 0.64 m/min	Flat x Concave Convex x Cylinder	Permanent Magnet (untouched)
Tank-like Robot [Versatrax100-Inuktun] 	2 roller chains	376 x 220 x 115 mm 4.5 kg 0.15 m/s	Flat x Concave x Convex Cylinder	Permanent Magnet (untouched)
4-Wheels robot [Wang_ICA2014] 	4 magnetic wheels (flexible frame)	352 × 215 × 155 mm 3 kg 0.32 m/s	Flat x Concave x Convex x Cylinder	Permanent Magnet
2-Wheels robot [Eich_MED2015] 	2 magnetic wheels	380 x 280 x 150 mm 0,67 kg 0.5 m/s	Flat x Concave x Convex x Cylinder	Permanent Magnet
Inch-worm robot [Ward2016] 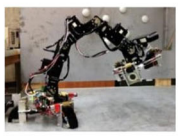	7-DOF-Inch worm	220 x 240 x 150 mm 18 kg 0.2 m/s	Flat x Concave Convex Cylinder	Permanent Magnet
Spider robot [Genki Sato2017] 	6 limbs-spider	600 x 600 x 250 mm 12 kg 0.2 m/min	Flat x Concave Convex Cylinder	Electromagnet

Fig. 2 The notable steel structure climbing robots

which cause the robot much heavier. Most existing designs have fixed distance between the magnet and surface, thus may not work on different types of surface contours. They might be difficult to apply on complicated structures of real bridges that require adaptable, light and effectively data collecting robot. Drones still get the limitation with energy issue and are able to perform visual/shallow inspection only.

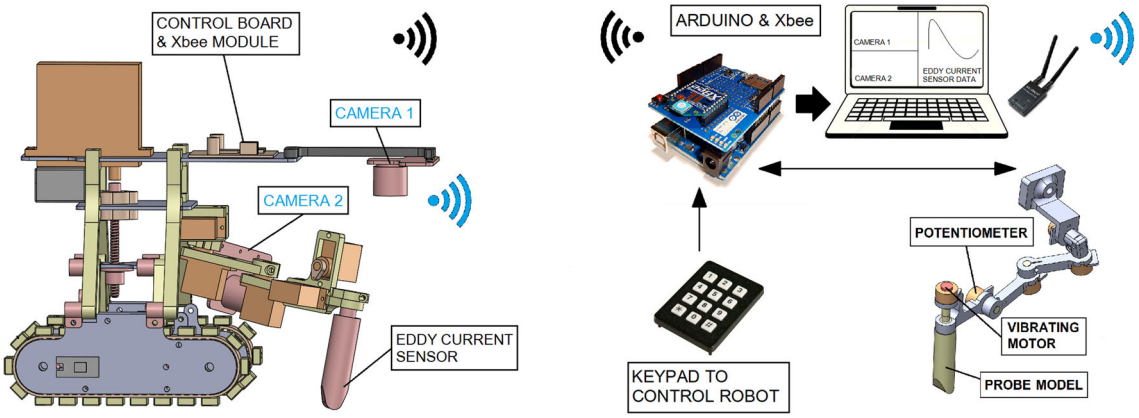

Fig. 3 System interface: Operator controls robot remotely from ground station via radio links. Xbee modules manage to send robot locomotion commands and receive data from sensor. A 5-DOF manipulator holding Eddy current sensor's probe is controlled by a haptic device while a keypad handles robot movement. Visual and sensor data are live on a PC screen

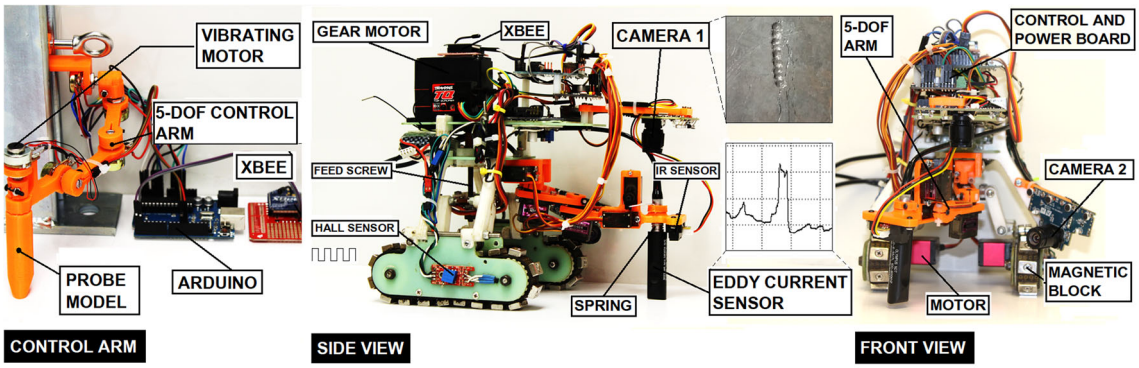

Fig. 4 Steel climbing robotic system. (Left) a simulated robotic arm on the ground station for remote control. (Middle) the side view of the robot. (Right) the front view of the robot. The robot equipped with both camera and Eddy current sensor for visual and non-destructive evaluation of the steel structure

Fig. 5 Roller chain with integrated Hall sensor and IR distance sensors. The IR sensor is served as a feedback of the PID control to regulate the reciprocating mechanism automatically on different contour surfaces. The detail of PID control function is described on Section 3.1 and Fig. 13

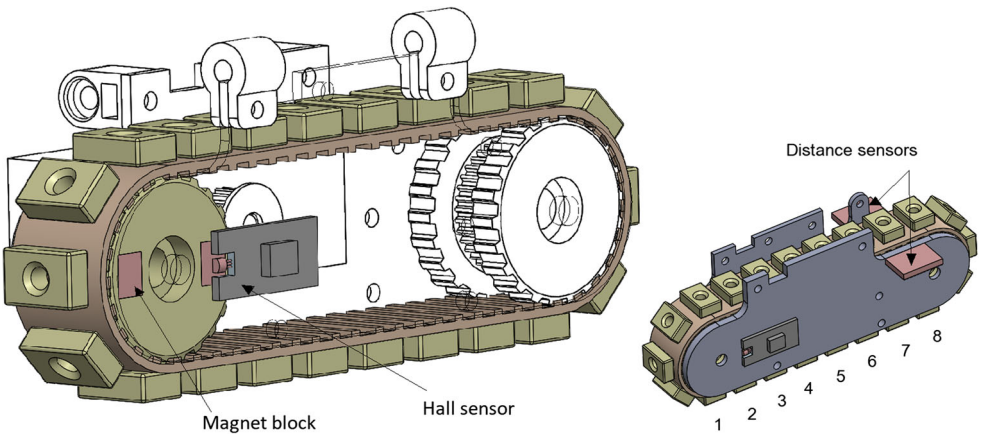

Table 1 Robot parameters

Length	163 mm
Width	145 mm
Height	198 mm
Weight	3 kg
Drive	2 motorized roller-chains and 1 motorized transformation

This paper presents a practical climbing robotic system to provide an efficient solution for steel bridge inspection. The robot can adapt to a wide range of different types of bridge surfaces (flat, curving, rough) and carry sufficient measurement devices including cameras and Eddy current sensor. The proposed small tank-like robot with reciprocating mechanism features various deformable 3D configurations, which can allow it to transition among steel structure members for efficient inspection. The robot utilizing adhesive force generated by permanent magnets is able to adhere well on steel structures while moving. The roller-chain design allows the robot to overcome obstacles including nuts, bolts, convex and concave corners. To demonstrate the robot's working principle, it has been deployed for climbing on more than 20 steel bridges. Video of this deployment can be seen in this link: https://ara.cse.unr.edu/?page_id=11.

The rest of the paper is organized as follows. Section 2 describes the overall robot design. Section 3 describes detailed mechanical design and magnetic force analysis of the robot when moving on surfaces with different inclinations. Section 4 shows various experiments to verify the proposed robot design and validate the magnetic force analysis. Finally, the conclusion and discussion of future work are presented in Section 5.

2 Overall Design

The overall design concept of a tank-like climbing robot is shown in Fig. 3 and the implementation of this design is shown in Fig. 4. The roller-chains embedded with permanent magnets for adhesive force creation enable the robot to adhere to steel surfaces without consuming any power. The control architecture of the robot consists of low-level and high-level controllers. The low-level controller handles tasks including (i) converting velocity and heading command from the high-level controller to Pulse Width Modulation (PWM) data to drive motors, and (ii) reading data from multiple sensors for navigation purposes. The high-level controller is embedded in an on board computer to enable data processing and ground station communication. Both controllers fuse sensor data to provide desired linear velocity and heading for the robot and acquire data from advanced sensors. Furthermore, the high-level controller sends data wirelessly to ground station for processing and logging.

The robot is equipped with various sensors for navigation as well as steel structure evaluation. There are two video cameras: one for capturing images of inspected surfaces, and the other one for guiding navigation of the robotic arm. There are two 5 DOF robotic arms: one on the robot for navigating the Eddy current sensor probe, and the other one for the operator/inspector, who can observe the camera's visual feedback then control this arm for manual operation purposes. The robot uses an IR sensor mounted on top of manipulator to give the feedback to operator by trigger a tiny vibrating motor on Haptic device. The robot has two roller-chains, and each roller-chain is integrated with two hall-effect sensors, which provide velocity feedback for PID speed controller. Figure 5 illustrates the sensor's mounting for each roller chain as we use two hall-effect sensors, which are mounted next to each other and close to robot's roller.

Since the magnet block inside each roller-chain will move when the robot moves, we can extract the velocity and traveling distance of each roller-chain after combining the data from these two hall-effect sensors. Additionally, an Inertial Measurement Unit (IMU) is used for the robot's localization. Moreover, to avoid falling off, the robot has IR (Infrared Radiation) sensors mounted in the robot to detect if a surface underneath exists.

For fatigue crack detection on steel structure, the Eddy current sensor's probe (Nortec 600) as shown in Fig. 6

Table 2 Motor parameters

	Moving motors	Transforming motor
Torque	1.2 N.m (2S Li-Po)	3.2 N.m
Speed	0.12 sec/ 60◦ (2S Li-Po)	0.15 sec/ 60◦ (2S Li-Po)
Length	40.13 mm	60.5 mm
Width	20.83 mm	30.4 mm
Height	39.62 mm	45.6 mm
Weight	71 g	156 g
Voltage	6-8.5V (2S Li-Po battery)	6-8.5V (2S Li-Po battery)

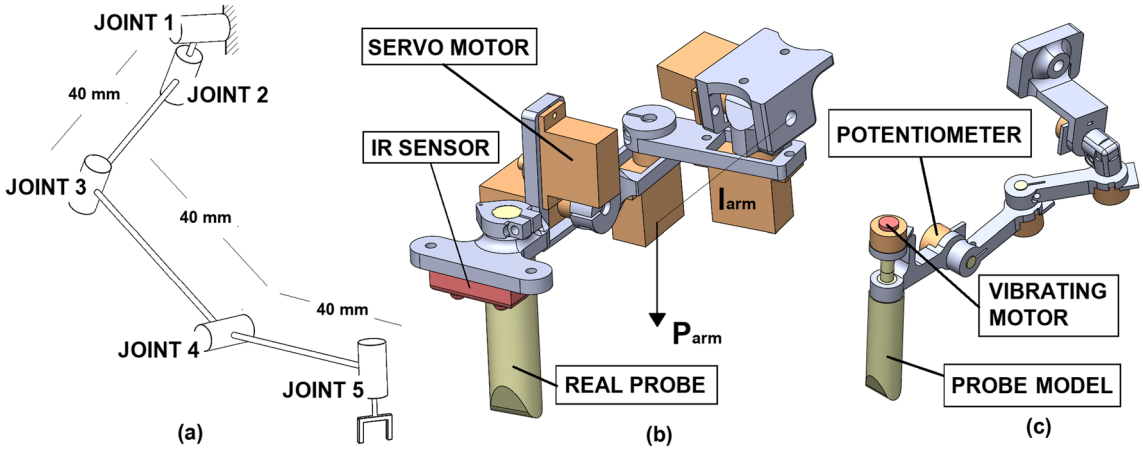

Fig. 6 **a** kinematic structure of 5-DOF arm; **b** executive arm integrating on the robot; **c** controlling arm for user operation in manual mode

is integrated with the robot. A mini 5-DOF robotic arm (Fig. 7a) is designed to hold and move the Eddy sensor's probe for data collection as demonstrated in Fig. 7b.

Maximum moment on joint 1 in Fig. 7a is described as

$$M_{arm} = P_{arm} * l_{arm}, \tag{1}$$

where $P_{arm} = 0.3kg$ is the total weight of the manipulator arm, $l_{arm} = 6cm$ is the distance from center of manipulator mass to joint 1, so $M_{arm} = 0.18N.m$. Five motors used are 0.25 N.m-torque-mini servos, which satisfy (1).

On ground station, the operator observes visual feedback from the camera and then controls a simulated arm (same scale as the one integrated with the robot) by holding and moving a probe model. The moving control signal is wirelessly sent via Xbee module to control the arm on the robot. Five joint's angles are obtained by potentiometers (Fig. 7c) then processed before sending required control angles to servo motors. An IR sensor is mounted on the Eddy current sensor's probe to determine whether the probe approaches the steel surface or not. When distance from IR sensor to the surface meets a calibrated number (45mm), a signal will be sent back to ground station to trigger a tiny vibrating motor on the simulated arm to enable Eddy data collection. Additionally, a pressure spring is placed between the probe and robotic arm to improve sensor's approaching. This design helps the sensor's probe to efficiently collect Eddy current data on complex surfaces such as weld, rough or curving.

3 Mechanical Design and Analysis

A tank-like robot mechanism design is proposed to take advantage of the flexibility in maneuvering. Two motors are used to drive two roller-chains, and another motor is used to drive the transformation of the robot to approach different contour surfaces. The robot's parameters are shown in Table 1 while the motor's parameters are listed in Table 2.

A roller-chain is designed to carry 22 Neodymium magnet blocks with poles on flat ends as presented in Fig. 4-front view. With each motion, there will be a maximum of

Fig. 7 (Left) Industrial Eddy current sensor Nortec 600; (Right) sensor probe for data collection

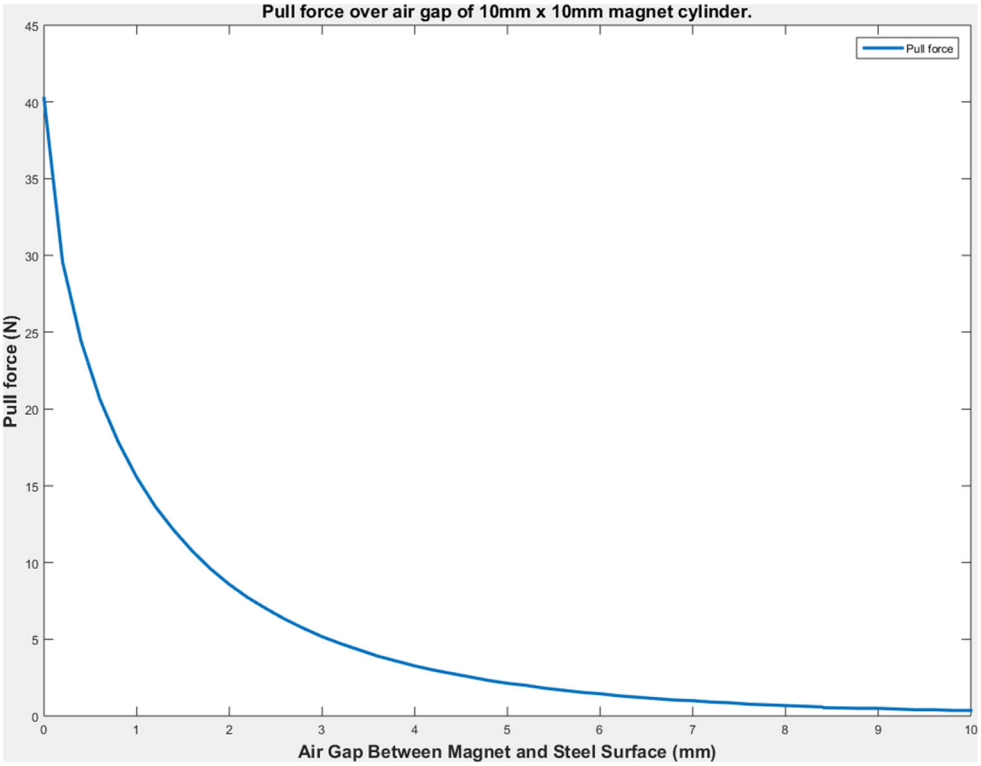

Fig. 8 Pull force over air gap of $10mm \times 10mm$ magnet cylinder

8 magnet blocks contacting the flat steel surface. According to [54], if there is a gap between magnet blocks and steel frame, the pull force is significantly affected. The characteristics of the used magnets ($15mm$ length $\times 10mm$ width $\times 5mm$ thickness magnet block) are described in Table 3 and pull force over air gap is shown in Fig. 8. Roller-chains are designed to enable the robot to overcome several real climbing scenarios including transitioning among surfaces with different inclination levels ($0 - 90°$ change in orientation) or getting rid of being stuck. A reciprocating mechanism has been added in order to transform the robot to adapt with different contour surfaces as shown in Fig. 9. The specifications of the robot's design is shown in Fig. 10.

Regarding magnetic force, denote that F_{mi} is magnetic forces created by each magnet blocks as shown in Fig. 5. At each moment there are a maximum 8 magnet blocks in the chain contacting the steel surface. Hence, we have the magnetic force created by each robot's roller-chain as: $\sum F_{m_j} (j = 1 : 8)$. Since the robot has two roller-chains,

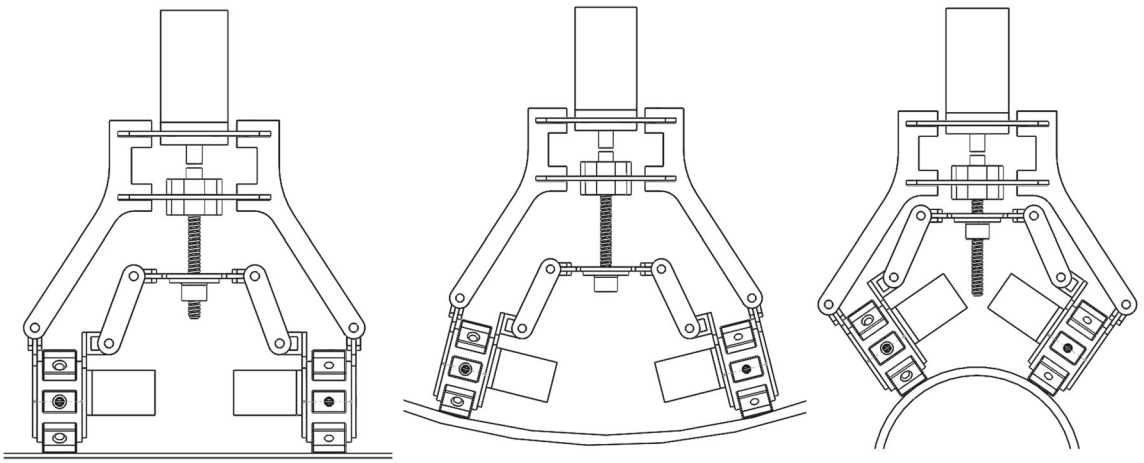

Fig. 9 Reciprocating mechanism for robot transformation on different surface: flat, negative curve and positive curve

Table 3 Pull Force (P^F) Over Air Gap of $15mm \times 10mm \times 5mm$ magnet block N35

Distance	PullForce P^F (Newton - N)		
(mm)	Magnet to steel plate	Between two steel plates	Magnet to magnet
0	39.7	73.1	39.7
1	17.1	29.8	22
2	10.1	17	15.3
3	6.4	10.5	11.1
4	4.3	6.9	8.4
5	2.9	4.6	6.4
6	2	3.2	5
7	1.5	2.2	4
8	1.1	1.6	3.2
9	0.8	1.1	2.5
10	0.6	0.8	2.1

the total magnetic adhesive force, F_m, created by these two roller-chains is:

$$F_m = 2 * \sum F_{m_j} (j = 1 : 8). \tag{2}$$

3.1 Robot Transformation Kinematics

Kinematics analysis of reciprocating mechanism is to calculate radius of steel cylinder (x), that the robot can climb on. Table 4 shows kinematic parameters while Fig. 9 presents kinematics of the robot, and Fig. 11 illustrates a general architecture of the robot's reciprocating mechanism.

From Fig. 12: $x = IC - CR$, in which, $IC = \frac{CF}{\cos\beta} = \frac{OF - OC}{\cos\beta} = \frac{b - \frac{f}{\cos\alpha}}{\cos\beta} = \frac{b}{\cos\beta} - \frac{f}{\cos\alpha\cos\beta}$; $CR = e - BC = e - f\tan\alpha$ with $\alpha + \beta = 90°$;

$$\rightarrow x = \frac{b}{\cos\beta} - \frac{b}{\cos\alpha\cos\beta} - e + f\tan\alpha. \tag{3}$$

$$\rightarrow b = \frac{\cos\alpha\cos\beta(f\tan\alpha - x - e)}{\cos\alpha - 1}. \tag{4}$$

Table 4 Kinematics parameters

b	72 mm
b1	45 mm
f	11 mm
e	55 mm
a	33.7 mm
XY	32 mm
γ	12°

From Fig. 11: $y = XZ = \sqrt{XY^2 - YZ^2}$, where $YZ = b_1 - OT \Leftrightarrow YZ = b_1 - OX\cos\phi$; $(\phi = \alpha - \gamma)$;

$$\rightarrow y = \sqrt{XY^2 - (b_1 - a\cos\phi)^2}. \tag{5}$$

From Eq. 4, $(b_1 = b - 27)$ Fig. 12 and Eq. 5 we get y = f(x)):

$$\rightarrow y = \sqrt{XY^2 - (\frac{\cos\alpha\cos\beta(f\tan\alpha - x - e)}{\cos\alpha - 1} - a\cos\phi - 27)^2}. \tag{6}$$

The feed screw mechanism has gear ratio is 1 : 19 with screw pitch is $0.8mm$.

From Eq. 6 and the designed gear ratio of 1:19, we can calculate radius x of the steel cylinder based on rotations of the transformation motor. The robot is designed to work on steel cylinders having a smallest radius from $+5cm$ to $-25cm$ with $7.5cm$ feed screw movement.

When the robot travels on different contour surfaces, reciprocating mechanism is driven automatically by the driving motor, which is based on the feedback from two IR distance sensors. A PID controller is applied to maintain the distance between the two sensors and the steel surface equally as illustrated on Fig. 13. The controller helps keep approaching area of permanent magnet with steel surface consistent.

3.2 Sliding Failure Investigation

To understand stability of the robot while climbing on steel structures, the sliding and turn-over failures as illustrated in Fig. 14a and b should be investigated.

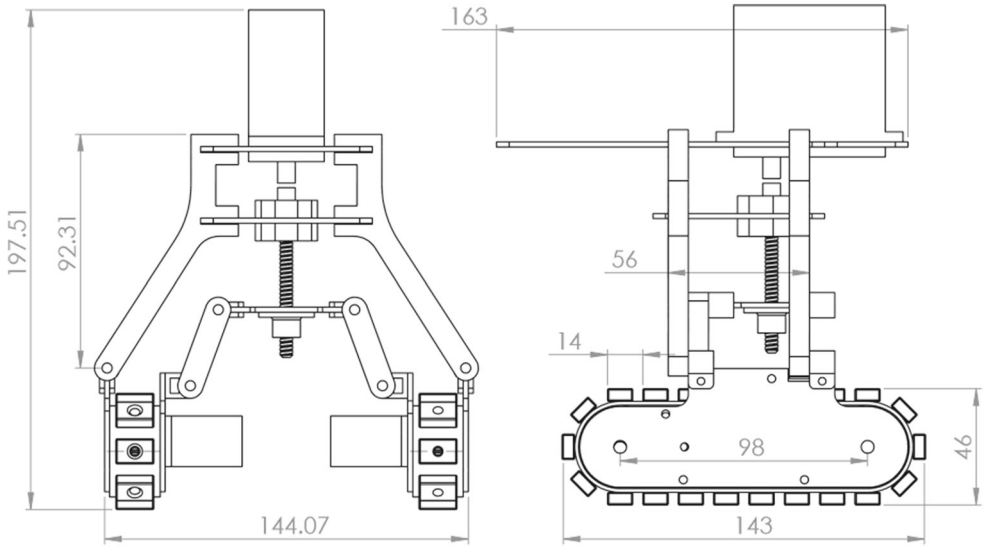

Fig. 10 Reciprocating mechanism for robot transformation and specifications of the robot's design (unit in mm)

In general case, based on the proposed design, the robot can climb on different shapes of structures (cylinder, cube or flat) with different inclination levels as shown in Fig. 15. In this analysis, we focus on basic working condition-flat surface to calculate the needed magnets and motor's parameters, then do experiments on different surfaces (curving, cube) in different conditions to find out optimal results.

Let P be the robot's total weight ($P = mg$, where m is the robot's mass, and g is the gravitational acceleration). Let F_m be the magnetic adhesive force, N be the reaction force, μ be the frictional coefficient, F_f be frictional force, and ϕ be the degree of inclination. Denote $\sum F$ as the total force applied to the robot. Based on Newton's second law of motion, $\sum F = 0$ when the robot stops.

When the robot climbs on top of an inclined surface (Fig. 15a), based on our previous work [30], we can obtain the magnetic adhesive force: $F_m = \dfrac{P \sin\phi}{\mu} - P\cos\phi$. Hence, the sliding failure can be avoided if the magnetic force satisfies the following condition:

$$F_m > \frac{P \sin\phi}{\mu} - P\cos\phi. \tag{7}$$

When the robot climbs underneath an inclined surface (Fig. 15b), we obtain: $F_m = \dfrac{P \sin\phi}{\mu} + P\cos\phi$. In this case,

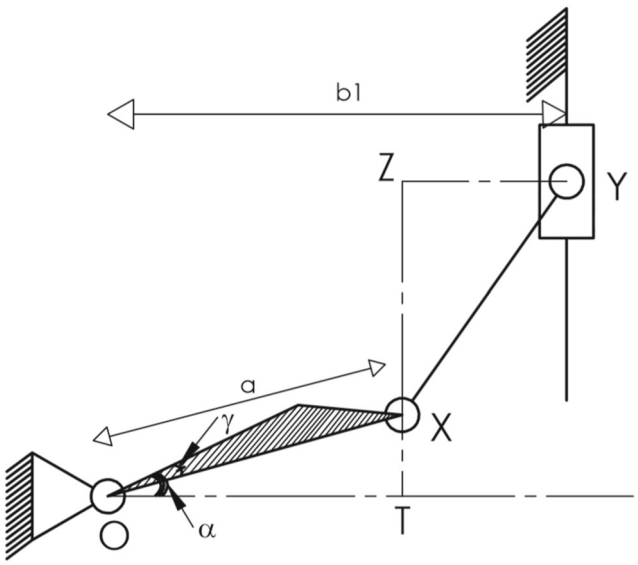

Fig. 11 Reciprocating mechanism: $a = 33.7mm$, $XY = 32mm$, and $\gamma = 12\circ$

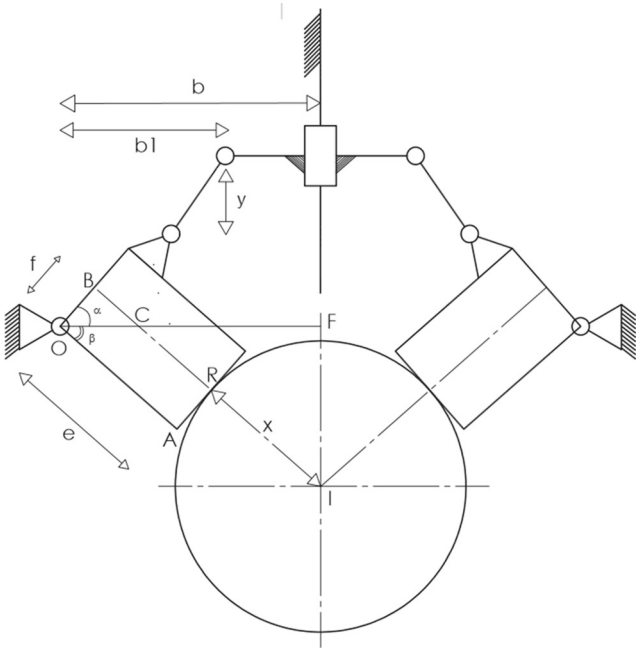

Fig. 12 Kinematics of the robot transforming mechanism: $b = 72mm$, $b_1 = 45mm$, $f = 11mm$, and $e = 55mm$

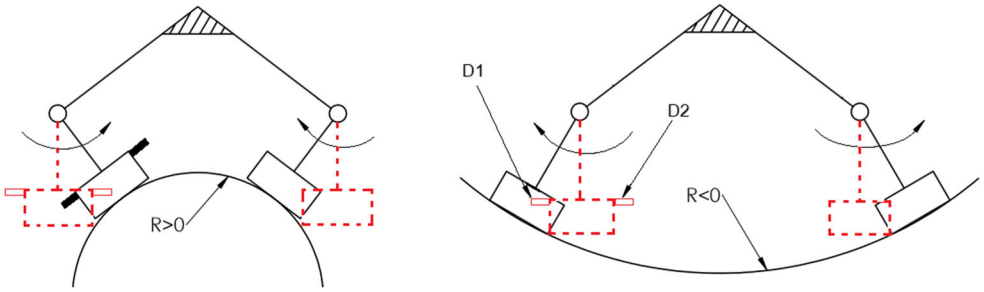

Fig. 13 Examples of different cases when the robot moves from flat to curved steel surface: (Left) positive curved surface; (Right) negative curved surface. A PID controller will be activated to keep the distance of two sensors D1 and D2 equally

the magnetic force should be

$$F_m > \frac{P \sin\phi}{\mu} + P\cos\phi. \tag{8}$$

When the robot climbs on a vertical surface ($\phi = 90^o$)

$$F_m > \frac{P}{\mu}. \tag{9}$$

From Eqs. 7, 8 and 9, to avoid sliding failure in any cases, the magnetic force should be

$$F_m > max\left\{\frac{P \sin\phi}{\mu} - P\cos\phi; \frac{P \sin\phi}{\mu} + P\cos\phi\right\}. \tag{10}$$

Since $0 < \phi \leq 90 \Rightarrow \cos\phi \geq 0$, the overall condition for avoiding sliding failure is

$$F_m > \frac{P \sin\phi}{\mu} + P\cos\phi. \tag{11}$$

Assume that the frictional coefficient μ between two roller-chains and steel surface is from [0.4−0.8], we see that $\left(\frac{\sin\phi}{\mu} + \cos\phi\right)$ decreases when μ increases, or we have:

$$0.4 \leq \mu \leq 0.8; 0 < \phi \leq 90$$
$$\Rightarrow max\left\{\frac{\sin\phi}{\mu} + \cos\phi\right\} = 2.5 \Rightarrow F_m \geq 2.5P.$$

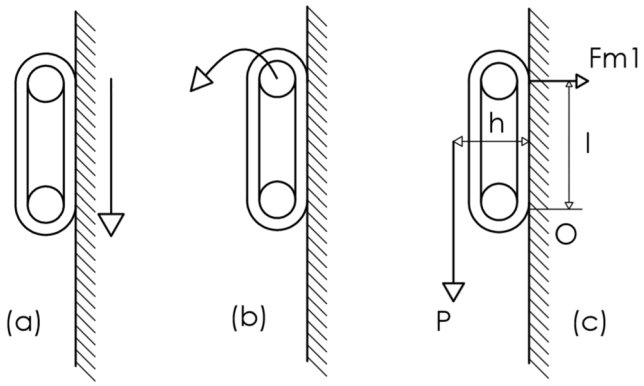

Fig. 14 **a** Sliding failure; **b** Turn-over failure; **c** Moment calculation at point O

In summary, the robot's magnetic adhesive force should be greater or equal to 2.5 of the robot's weight. The value of one permanent magnet, where $n = 8$ is the maximum number of magnet blocks contacting to the steel surface, satisfies the condition (12).

$$F_{m_j}(j = 1:n) \geq \frac{2.5P}{n}. \tag{12}$$

3.3 Turn-over Failure Investigation

Let l be the distance between first and last magnet block contacting to the surface, and h be the distance between the center of mass to the surface (Fig. 14c). Moment at point O (the point that the first magnet block contacts the steel surface) is calculated as follows:

$$\sum M = P * h - 2F_{m_1} * l = 0 \Leftrightarrow F_{m_1} = \frac{P * h}{2l}.$$

To avoid turn-over failure, the magnetic force of the first contacting magnet block:

$$F_{m_1} > \frac{P * h}{2l}. \tag{13}$$

From Eq. 13, to avoid the failure we can lower $\frac{h}{l}$, which means making the robot's center of mass closer to the steel surface. In the proposed design (Fig. 10), $h = 4.6$cm, and the total robot height $h_r = h + 9.231cm = 19.751$cm. Therefore, to avoid both sliding and turn-over failures, the robot's magnetic force of each magnet block should satisfy:

$$F_{m_j}(j = 1:n) > max\left\{\frac{2.5P}{n}; \frac{P * h_r}{2l}\right\}. \tag{14}$$

Following the proposed design, $P = 30$N, $n = 16$ magnet blocks (each roller-chain has maximum 8 magnet blocks contacting the steel surface), $l = 9.8$cm, or $F_{m_j}(j = 1:16) > max\left\{\frac{2.5 * 3}{16}; \frac{3 * 19.751}{2 * 9.8}\right\} > 3(N)$. We conducted

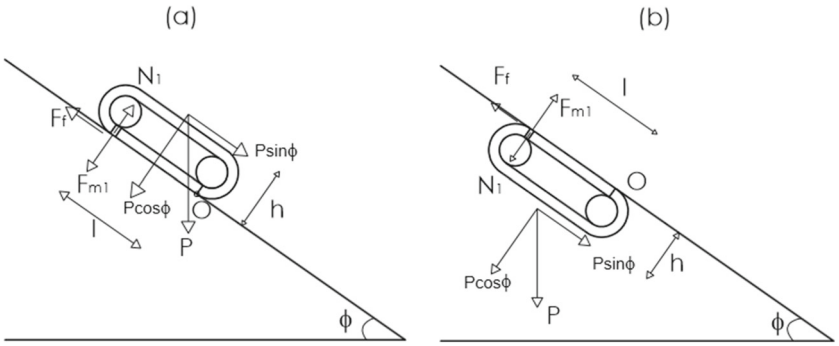

Fig. 15 **a** Climbing on top inclined surface; **b** Climbing underneath inclined surface

some tests as discussed in Section 4.1 to make sure the proposed design satisfied this condition.

3.4 Magnetic Force Analysis on Curved Surfaces

The previous analysis is only applied when robot moves on a flat steel surface. However, there are also structures, which have curving surface, so the following analysis will help determine the impact of curving surface on magnetic force created by the robot.

An experiment conducted on different steel cylinder shapes with real condition to verify the performance of magnet blocks working on curving surfaces is shown on Table 5.

Table 5 Average Pull force (P^F) over inside and outside steel cylinders of $15 \times 10 \times 5mm$ magnet block $N35$

Diameter (mm)	PullForce P^F (Newton - N)
100	13.5
200	15.5
300	16.2
400	17.4
500	19.3
600	20.9
700	23.2
800	25.4
900	28
flat	32.5
−900	24.4
−800	21.2
−700	19.7
−600	18.3
−500	17.2

Experiment was conducted on $5mm$ thickness steel with $0.2mm$ paint on surface

The minimum pull-force is $13.5N$ at $100mm$ diameter steel cylinder, and this means that it is always greater than $3N$, the required force, as showed in Eq. 14.

3.5 Motor Torque Analysis

Apart from the magnetic force analysis, we have conducted another analysis to determine the appropriate motor to drive the robot. In order to make the robot move, the force created by the motor should win the adhesive force of the last permanent magnet and the steel surface. As shown in Fig. 16, denote M as the torque of one motor, Q is rotation fulcrum, i is the arm from F_{m_j} to Q. Assume that the total driving force of the robot is the sum of two motor's forces, the required moment is satisfied:

$$M > h_r * \frac{P \sin\phi}{2} + F_{m_j}(j = 1 : n) * i.$$

When the robot moves on a vertical surface, maximum $\phi = 90^0$

$$M > h_r * \frac{P}{2} + F_{m_j}(j = 1 : n) * i. \quad (15)$$

$\rightarrow M > 3.16(N.m)$ with $h_r = 19.751cm, P = 30N, g = 9.8, F_{m_n} = 39.7N$ (obtained this number from the magnet's datasheet), $i = 0.5cm$. The selected moving motor moment is $1.2N.m$ and gear ratio is $7 : 20$, hence the moment of a robot roller-chain is $3.43N.m$, which satisfies (15).

Regarding transformation mechanism as shown in Fig. 17, when the robot moves from flat surface to curving surface or reversing, the transforming mechanism works to make sure that the roller-chains contact steel surfaces with best condition. The transformation motor through mechanical system creates moment (M) to release magnet blocks from steel surface. However, the calculation gear ratio of reciprocating mechanism is not simple due to its non-linearities, as showed in Eq. 5. We choose the special case when friction is strongest to calculate the moment of the transforming motor (powering feed screw mechanism).

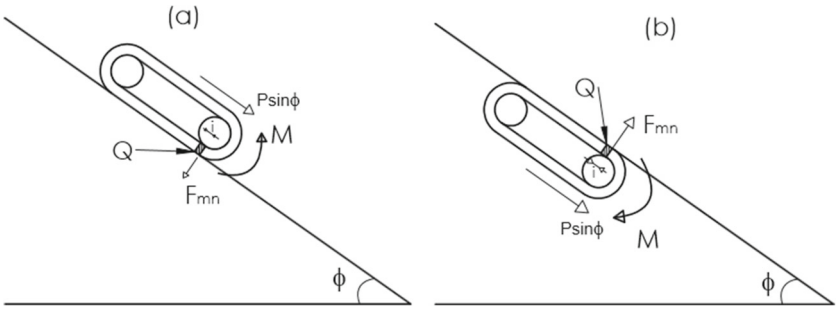

Fig. 16 **a** Robot moves on top of inclined surface; **b** Robot moves on bottom of inclined surface

The moment has to satisfy:

$$M > F_f * e \Leftrightarrow M > e * (k.N) \Leftrightarrow M > e * k(P + F_m).$$

$$\Rightarrow M > e * k(P + nF_{m_j}(j = 1 : n)). \quad (16)$$

From Eq. 5 and kinematics parameter of reciprocating mechanism, it is straight forward to calculate the gear ratio in this case. The ratio $\alpha : y$ is approximately $1° : 1mm$. Besides, the ratio of $a : e = 1 : 1.7$, and the gear ratio of the feed screw is $0.8mm : 360°$. As result, a total gear ratio of whole system is $26.5 : 1$. From Eq. 16 and assumption that system efficiency is 80%, the required moment of motor is $> 1.375N.m$. The selected transformation motor with $3.2N.m$ is satisfied.

When the robot travels on curving surfaces, reciprocating mechanism is driven automatically by driving the motor based on IR sensor signals. A PID controller is also applied to maintain the distance between the IR sensor and the surface. This is to keep approaching area of permanent magnets with the steel surface consistent.

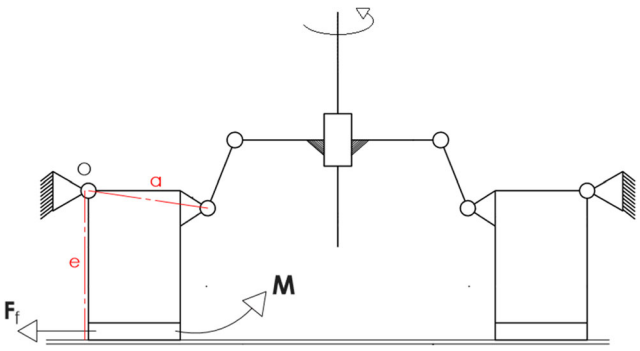

Fig. 17 Transformation mechanism with 7 joints to create climbing flexibility of the robot

4 Robot Deployment

To evaluate design and performance of the robot, experiments for evaluating the magnetic force created by roller-chains have been conducted. The ability of climbing and failure avoidance were tested. During the test, a Lipo battery (2 cells) 7.4V 900 milliampere-hour (mAh) is used to power the robot for about 1 hour of working. One laptop which can connect to a wireless LAN is used as a ground station. The robot's mass $m = 3kg$, and if we assume that the gravitational acceleration $g = 10m/s^2$, the total weight of the robot is approximately $P = mg = 30N$. Since $15mm \times 10mm \times 5mm$ magnet blocks are used, the total magnetic force is calculated as

$$\begin{cases} F_{m_j}(j = 1 : 8) = 39.7(N) \\ F_m = 2 * 8 * F_{m_j} = 635.2(N) \end{cases} \quad (17)$$

which satisfies magnetic force condition as presented in Eq. 14.

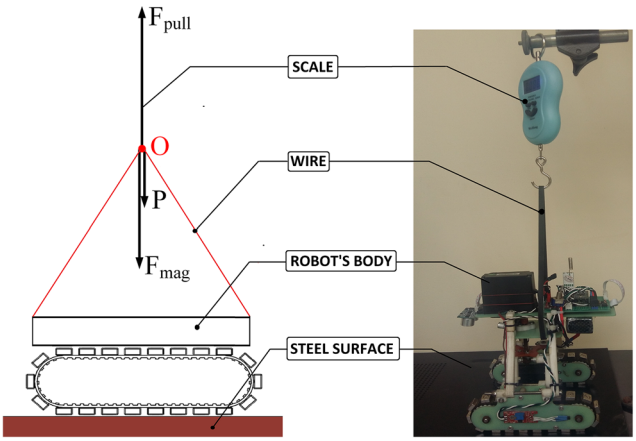

Fig. 18 Experimental setup for magnetic force measurement

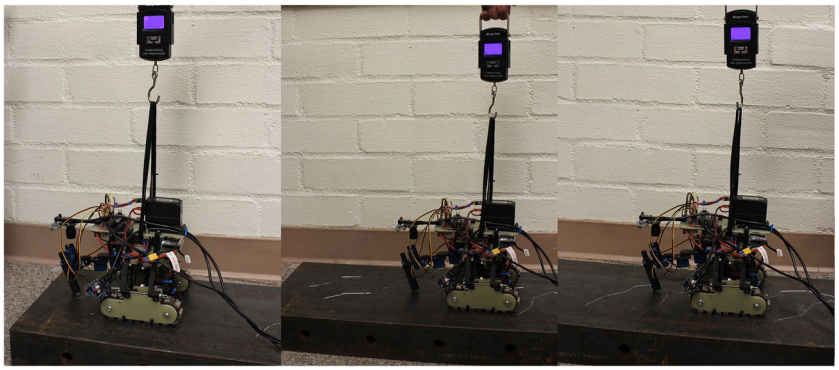

Fig. 19 Adhesive force measurement in dynamic condition on non-coated flat surface (robot moves from right to left images)

4.1 Adhesive Force Measurement

4.1.1 Static Condition

In order to measure the adhesive force created by permanent magnet, we have setup an environment as shown in Fig. 18. The robot's body - whose mass is $m = 3kg$ - is placed on top of a flat steel surface while it is connected to a scale through an inelastic wire. We create a pull force onto the scale trying to lift the robot off the surface. At the time the robot is about to be off the surface, the force applied to the scale is equal to the sum of robot's weight and the magnetic pull force. Denote F_{pull} as the force we applied onto the scale, M is the value shown on the scale while P is the weight of robot's body, and F_{mag} is the magnetic force. With $g = 10m/s^2$, $P = mg = 30N$ and $F_{pull} = Mg = 10M$, we can calculate magnetic adhesive force as follows

$$F_{pull} = P + F_m \Rightarrow F_m = F_{pull} - P$$
$$\Rightarrow F_{mag} = 10M - 3(N). \quad (18)$$

4.1.2 Dynamic Condition

We also measure the adhesive force of the robot in moving state as shown Fig. 19 (robot moves from right to left). Each measurement is conducted three times as shown in Fig. 20. In average, the adhesive force in dynamic condition is lower than approximately 10% comparing to static state.

Multiple tests have been conducted to measure the pull force when the robot's body is placed on different surfaces. The first test is on a flat non-coated steel surface, the second one is on a flat coated steel surface while the third test is on curve coated steel surfaces (positive and negative sides) with diameters (D) ranging from $100mm$ to $900mm$. All the tests are executed three times, and the results are presented in Figs. 21 and 22.

According to Eq. 14, the magnetic force for each magnet block should be $F_{m_j}(j = 1 : n) > 3(N)$ to avoid sliding and turn-over failure. Since at each time the robot has 16 magnet blocks, which physically contact the steel surface, the total required adhesive force should be greater than $3 \times 16 = 48(N)$. We can see that in Figs. 21 and 22 the minimum magnetic force is $115(N)$, which is much greater than the required one, $48(N)$ with safety factor is around 2.5. Therefore the robot adheres well on both coated/non-coated flat and curving surfaces.

4.2 Robot Field Deployment

The outdoor experiments and robot deployments are conducted on more than 20 steel bridges. Due to limited space, only some typical climbing examples are shown in Figs. 23–27. The steel structures have different thicknesses of paint coated on steel surfaces. Some paint-coated steel

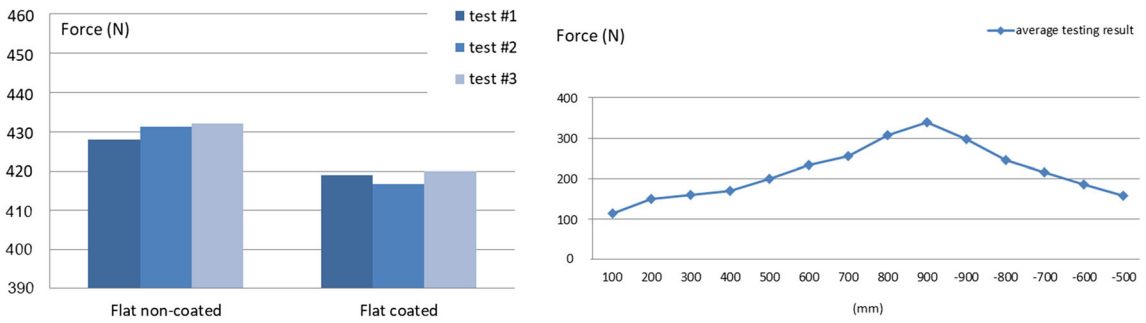

Fig. 20 (Left) testing result on flat surfaces, (right) testing result on coated curving surfaces (cylinder tubes)

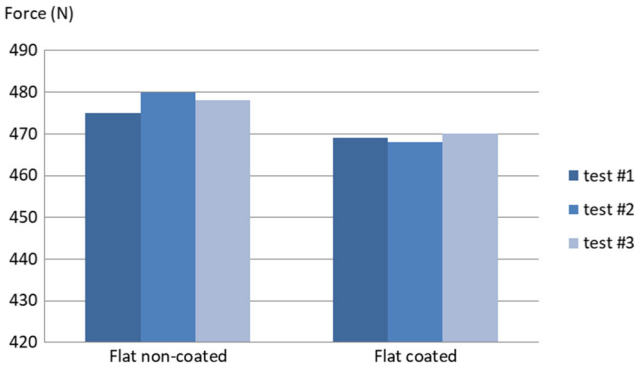

Fig. 21 Magnetic force measurements on coated and non-coated flat steel surface

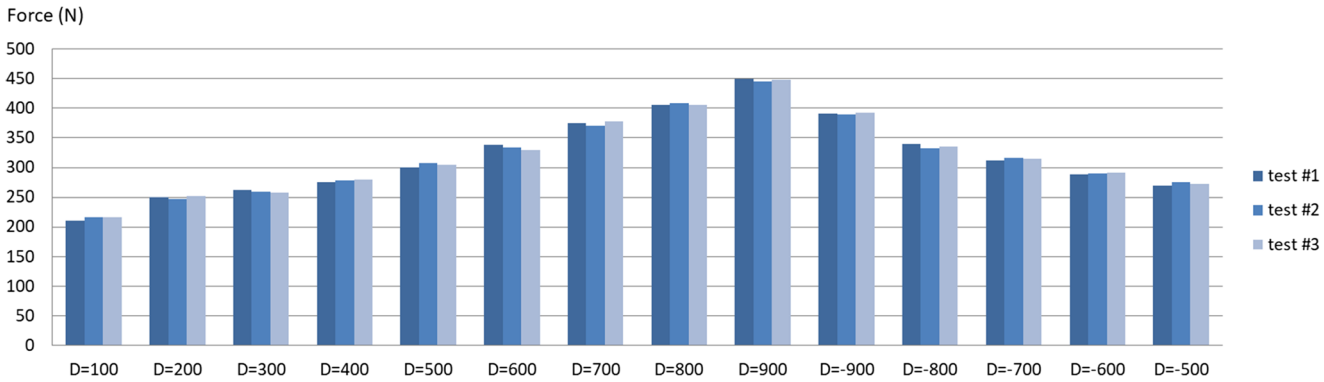

Fig. 22 Magnetic force measurements on curving steel surface with diameters (D) ranging from 100*mm* to 900*mm*

Table 6 Statistical result

Structrural parameters	Decription
Thinnest steel surface	1 (mm)
Smallest steel cylinder diameter	100 (mm)
Thickest coated paint	4 (mm)
Highest nut or bolt area	12 (mm)

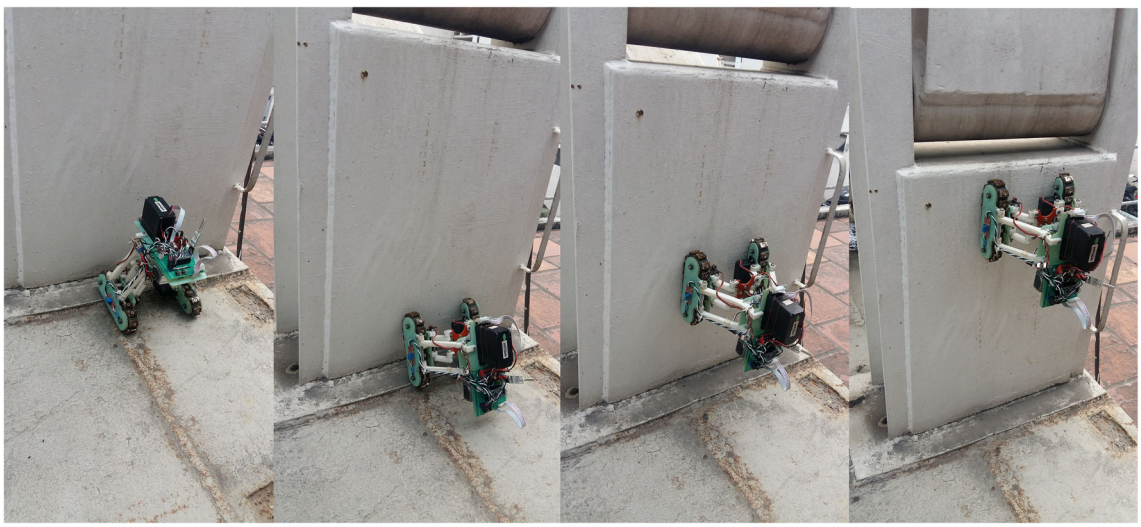

Fig. 23 Adhesive and climbing test on a thick paint-coated steel structure: flat surface

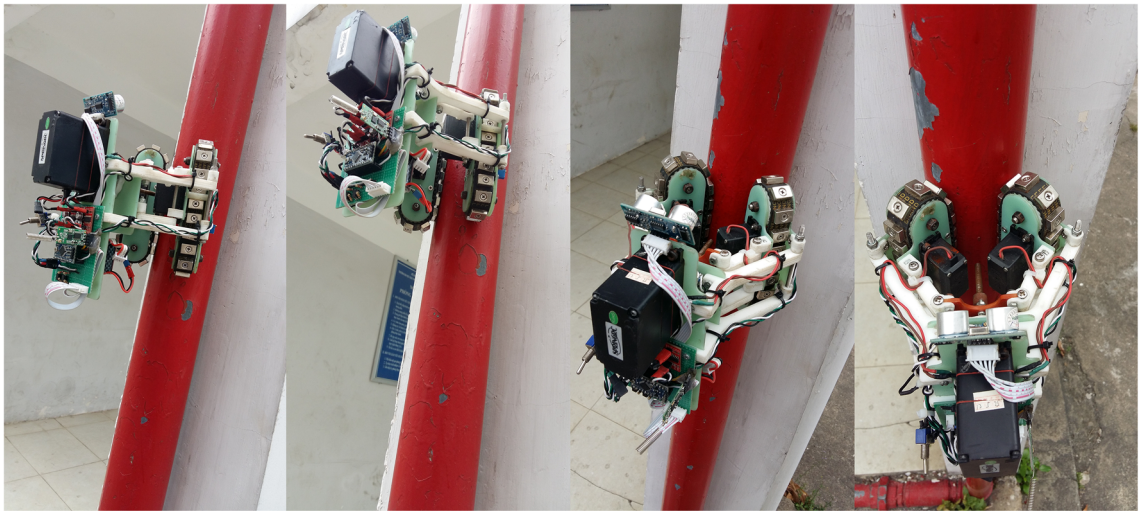

Fig. 24 Adhesive and climbing test on a thin paint-coated steel structure: cylinder shape D=100mm

surfaces are very rusty, some are not clean, and some others are still in fine condition (minor-rusty). Statistical results with description of specifications that the robot can work with is presented in Table 6.

During the experiments, the climbing capability tests are done on steel bridges and steel structures, and on with coated or unclean surfaces as seen on Figs. 23, 24, 25, 26 and 27. The robot is able to adhere very well on these steel structures while climbing with maximum speed is 200 mm/s during 1 hour. Even for the case of curving surface (Figs. 24 and 25), the robot can still adhere tightly to the steel structures while performing the climb. For rusty steel surfaces, it also shows strong climbing capability (Fig. 27). However, in some very tough conditions, such as bird drops or high nuts, the robot might loose adhesive force and can not pass these areas. Robot deployments can be seen in the submitted video and the ARA lab link: https://ara.cse.unr.edu/?page_id=11 or youtube link: https://youtu.be/1Wl9Trd3EoM.

The robot is controlled to move and stop at every certain distance (e.g. 12cm) to capture images of steel surfaces and do closer investigation on potential crack areas, then send to the ground station. To enhance steel surface inspection, acquired images are then stitched together to produce an overall image of steel surfaces as shown in Fig. 28. The image stitching is followed by our previously developed algorithm [41].

In addition to the visual data collection, the robot also collects Eddy current data as shown in Fig. 29. The survey is conducted on a 170 x 70 mm area, which contains some

Fig. 25 Adhesive and climbing test on a thin paint-coated steel structure: cylinder shape D=250mm

Fig. 26 Adhesive and climbing test on a thick paint-coated steel bridge: flat surface

crack areas as shown in Fig. 30a. The robotic arm holds the Eddy current sensor's probe and performs a zig-zag path consisting of four lines. Figure 30b-e shows raw signals collected in a 13-seconds time frame for each line. We can see from these plots that at the crack areas, the signal amplitude is higher. For the ease of illustration, a color coded map is built as shown in Fig. 31, and we can see that the Eddy current condition/fatigue crack map has defect areas (red/yellow color) correlating very well with the crack areas on the image.

5 Conclusion and Future Work

This paper presents a new development of a tank-like robot, which is capable of climbing on different steel structure shapes to perform inspection and evaluation. The robot design is implemented and validated on climbing on more than twenty different steel bridges. During the tests, the robot is able to firmly adhere on steel structures with various inclination levels. Rigorous analysis of magnetic adhesive force has been performed to confirm that the robot is able to adhere to both flat and curving steel surfaces in various conditions (coated, non-coated and/or rusty). Moreover, motor torque analysis to make sure the robot can win the magnetic adhesive force to move on steel surface is presented. Various experiments have been conducted including magnetic force measurement, indoor and outdoor climbing tests in order to validate the force analysis as well as the climbing capability of the robot. The results show that when the magnetic adhesive force requirement is met, the robot is able to move and transition safely between

Fig. 27 Adhesive and climbing test on a rusty paint-coated steel bridge: flat structure with bolts/nuts

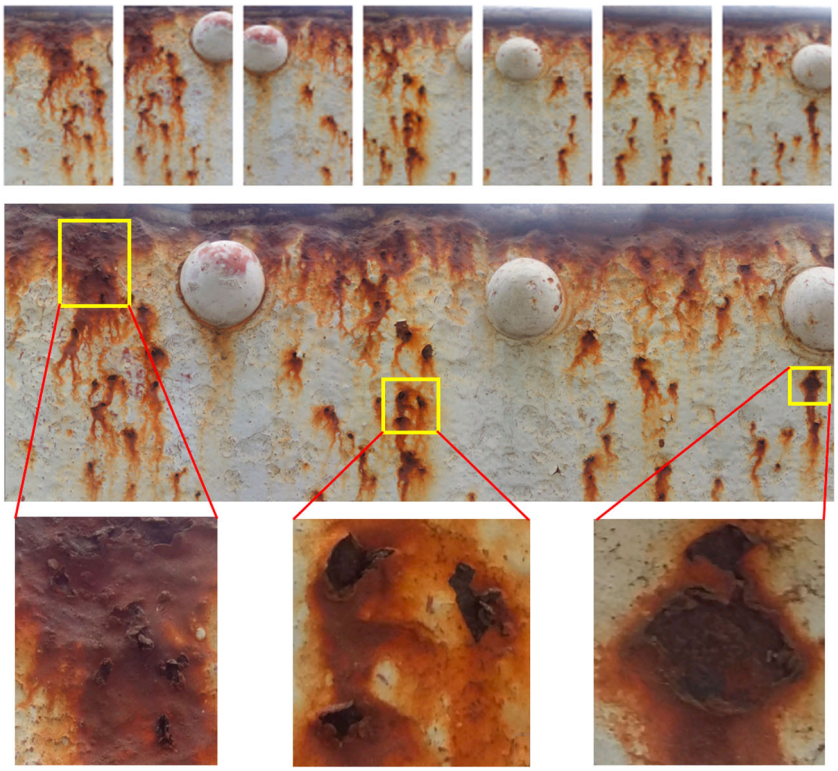

Fig. 28 Images stitching result: (Top) 7 individual images taken by the robot climbing on a bridge in Fig. 27; (Middle) Stitching image result from those 7 individual images; (Bottom) Closer look (zoom-in) at some areas, which has serious rusty condition with holes on the surface

steel surfaces without any failures. Several sensors are integrated to support the robot's navigation as well as data collection. The rigorous magnetic force analysis can serve as a framework to calculate and design different types of steel inspection robots in the future. Inspection data (Eddy current and visual) is collected and transferred to ground station for visualization and processing.

Further works can be focusing localization on using odometry, IMU and visual data, and implementation of map construction methods as well as visual deep learning-based crack detection algorithms. The robot can be further equipped with other NDE sensors (e.g., thermal sensors) for more in-depth inspection of steel structures. Additionally, the robot can be further improved to move in circumfer-

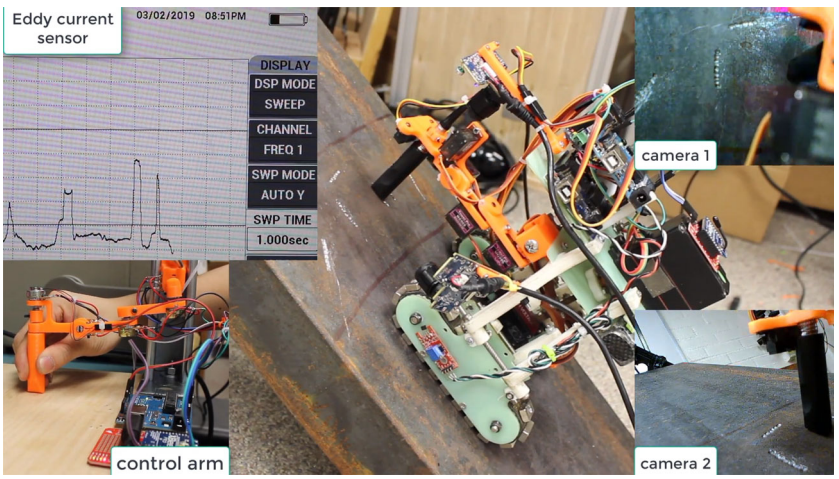

Fig. 29 Crack surveying process. Visual data is acquired by camera 1 (top-right image). Operator controls Eddy current sensor's probe remotely by a haptic system (control arm: bottom-left image) with closer view from camera 2 (bottom-right image). Eddy current sensor measures depth of crack (top-left image), more detail in Fig. 30

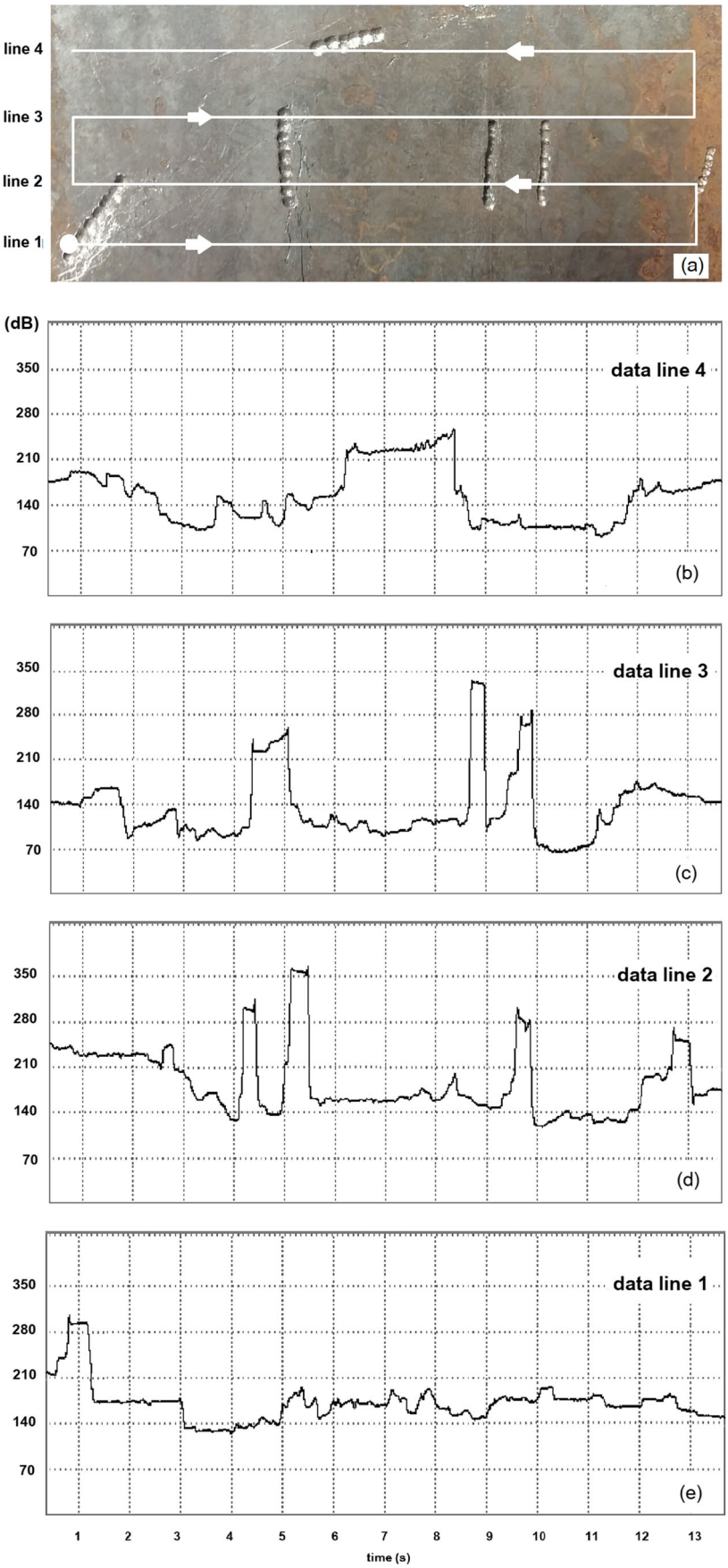

Fig. 30 **a** Probe path; **b** line 4 data; **c** line 3 data; **d** line 2 data; **e** line 1 data

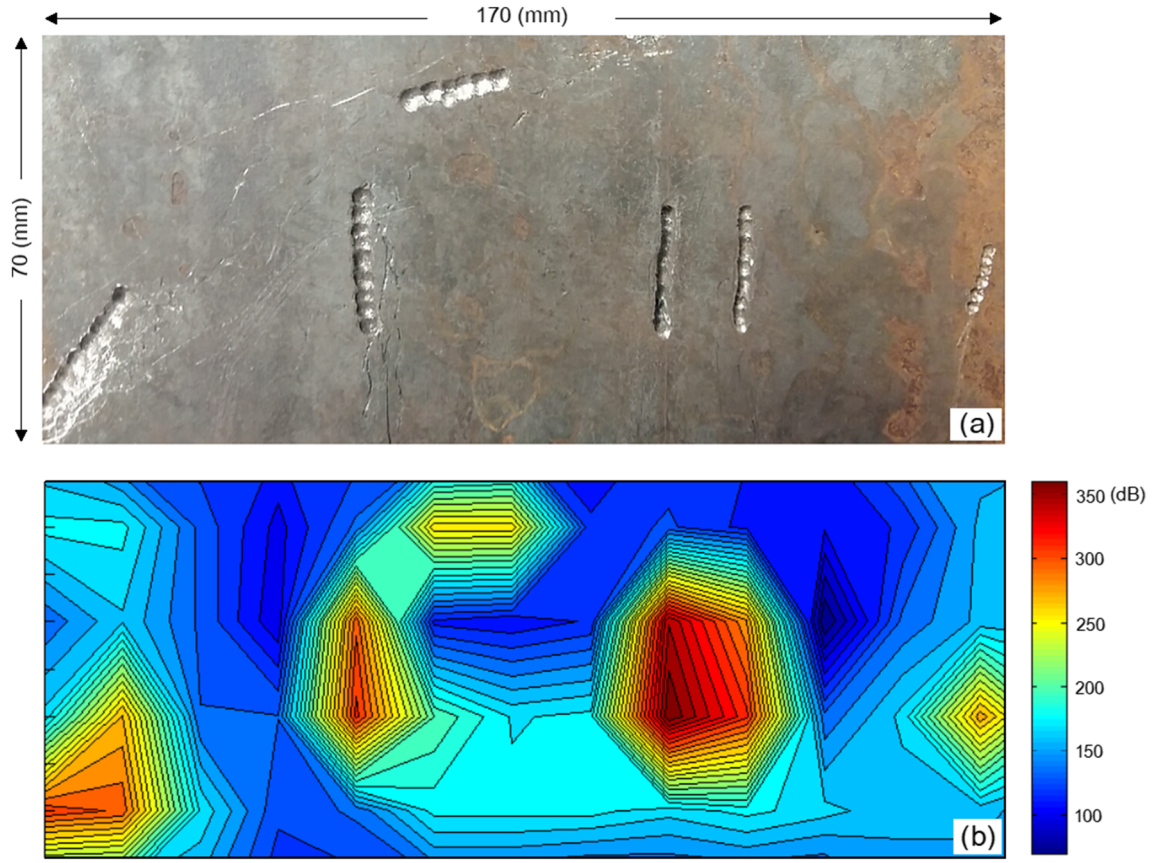

Fig. 31 **a** Image of an inspected area with cracks on it; **b** Fatigue crack map from Eddy current sensor showing defect areas with red/yellow color, corresponding well with the crack areas on the image

ential directions on small diameter cylinder-like objects. Beyond steel bridge inspection, this robot can be applied for inspection of oil tank, pipeline, and other civil facilities. A collaborative algorithm can be developed to employ multiple robots for faster inspecting a large steel bridge or structure.

Acknowledgements This work is supported by the U.S. National Science Foundation (NSF) under grants NSF-CAREER: 1846513 and NSF-PFI-TT: 1919127, and the U.S. Department of Transportation, Office of the Assistant Secretary for Research and Technology (USDOT/OST-R) under Grant No. 69A3551747126 through INSPIRE University Transportation Center, and the Vingroup Innovation Foundation (VINIF) in project code VINIF.2020.NCUD.DA094. The views, opinions, findings and conclusions reflected in this publication are solely those of the authors and do not represent the official policy or position of the NSF, the USDOT/OST-R and any other entities.

References

1. FHWA: U.S Department of transportation highway administration, national bridge inventory data. http://www.fhwa.dot.gov/bridge/nbi.cfm (2019)
2. Stark, T.D., Benekohal, R., Fahnestock, L.A., LaFave, J.M., He, J., Wittenkeller, C.: I-5 skagit river bridge collapse review. J. Perform. Constr. Facil. **30**(6), 04016061 (2016)
3. McCrea, A., Chamberlain, D., Navon, R.: Automated inspection and restoration of steel bridges – a critical review of methods and enabling technologies. Autom. Constr. **11**(4), 351–373 (2002)
4. La, H.M., Dinh, T.H., Pham, N.H., Ha, Q.P., Pham, A.Q.: Automated robotic monitoring and inspection of steel structures and bridges. Robotica **37**(5), 947–967 (2019)
5. Fischer, W., Tâche, F., Siegwart, R.: Magnetic wall climbing robot for thin surfaces with specific obstacles. In: Laugier, C., Siegwart, R. (eds.) Field and Service Robotics: Results of the 6th International Conference, pp. 551–561. Springer, Berlin (2008)
6. Fischer, W., Caprari, G., Siegwart, R., Moser, R.: Locomotion system for a mobile robot on magnetic wheels with both axial and circumferential mobility and with only an 8-mm height for generator inspection with the rotor still installed. IEEE Trans. Ind. Electron. **58**(12), 5296–5303 (2011)
7. Ratsamee, P., Kriengkomol, P., Arai, T., Kamiyama, K., Mae, Y., Kiyokawa, K., Mashita, T., Uranishi, Y., Takemura, H.: A hybrid flying and walking robot for steel bridge inspection. In: IEEE Inter. Symp. on Safety, Security, and Res. Robo., pp. 62–67 (2016)
8. Wang, H., Yamamoto, A.: Analyses and solutions for the buckling of thin and flexible electrostatic inchworm climbing robots. IEEE Trans. Robot. **33**(4), 889–900 (2017)
9. Shen, W., Gu, J., Shen, Y.: Permanent magnetic system design for the wall-climbing robot. In: IEEE International Conference Mechatronics and Automation, 2005, vol. 4, pp. 2078–2083 (2005)

10. Mazumdar, A., Asada, H.H.: Mag-foot: A steel bridge inspection robot. In: 2009. IROS 2009. IEEE/RSJ International Conference on Intelligent Robots and Systems, pp. 1691–1696 (2009)
11. Wang, R., Kawamura, Y.: A magnetic climbing robot for steel bridge inspection. In: 2014 11th World Congress on Intelligent Control and Automation (WCICA), pp. 3303–3308 (2014)
12. Tche, F., Fischer, W., Caprari, G., Siegwart, R., Moser, R., Mondada, F.: Magnebike: A magnetic wheeled robot with high mobility for inspecting complex-shaped structures. J. Field Robot. **26**(5), 453–476 (2009)
13. Pack, R.T., Christopher, J., Kawamura, K.: A rubbertuator-based structure-climbing inspection robot. In: 1997. Proceedings., 1997 IEEE International Conference on Robotics and Automation, vol. 3, pp. 1869–1874 (1997)
14. Abderrahim, M., Balaguer, C., Gimenez, A., Pastor, J.M., Padron, V.M.: Roma: a climbing robot for inspection operations. In: 1999. Proceedings. 1999 IEEE International Conference on Robotics and Automation, vol. 3, pp. 2303–2308 (1999)
15. Leibbrandt, A., Caprari, G., Angst, U., Siegwart, R.Y., Flatt, R.J., Elsener, B.: Climbing robot for corrosion monitoring of reinforced concrete structures. In: Applied Robotics for the Power Industry (CARPI), the 2nd Intern. Conf. on, pp. 10–15 (2012)
16. Leon-Rodriguez, H., Hussain, S., Sattar, T.: A compact wall-climbing and surface adaptation robot for non-destructive testing. In: 2012 12th International Conference on Control, Automation and Systems (ICCAS), pp. 404–409 (2012)
17. San-Millan, A.: Design of a teleoperated wall climbing robot for oil tank inspection. In: 2015 23th Mediterranean Conference on Control and Automation (MED), pp. 255–261 (2015)
18. Shen, W., Gu, J., Shen, Y.: Proposed wall climbing robot with permanent magnetic tracks for inspecting oil tanks. In: IEEE International Conference Mechatronics and Automation, 2005, vol. 4, pp. 2072–2077 (2005)
19. Tavakoli, M., Viegas, C., Marques, L., Pires, J.N., deAlmeida, A.T.: Omniclimbers: Omni-directional magnetic wheeled climbing robots for inspection of ferromagnetic structures. Robot. Auton. Syst. **61**(9), 997–1007 (2013)
20. Eich, M., Vgele, T.: Design and control of a lightweight magnetic climbing robot for vessel inspection. In: The 19th Mediterranean Conf. on Control Automation, pp. 1200–1205 (2011)
21. Caprari, G., Breitenmoser, A., Fischer, W., Hurzeler, C., Tache, F., Siegwart, R., Nguyen, O., Moser, R., Schoeneich, P., Mondada, F.: Highly compact robots for inspection of power plants. J. Field Robot. **29**(1), 47–68 (2012)
22. Cho, K.H., Kim, H.M., Jin, Y.H., Liu, F., Moon, H., Koo, J.C., Choi, H.R.: Inspection robot for hanger cable of suspension bridge: Mechanism design and analysis. IEEE/ASME Trans. Mechatron. **18**(6), 1665–1674 (2013)
23. Zhu, D., Guo, J., Cho, C., Wang, Y., Lee, K.: Wireless mobile sensor network for the system identification of a space frame bridge. IEEE/ASME Trans. Mechatron. **17**(3), 499–507 (2012)
24. Lee, G., Wu, G., Kim, J., Seo, T.: High-payload climbing and transitioning by compliant locomotion with magnetic adhesion. Robot. Auton. Syst. **60**(10), 1308–1316 (2012)
25. Seo, T., Sitti, M.: Tank-like module-based climbing robot using passive compliant joints. IEEE/ASME Trans. Mechatron. **18**(1), 397–408 (2013)
26. Wang, R., Kawamura, Y.: A magnetic climbing robot for steel bridge inspection. In: Proceeding of the 11th World Congress on Intelligent Control and Automation, pp. 3303–3308 (2014)
27. Guo, J., Liu, W., Lee, K.M.: Design of flexonic mobile node using 3d compliant beam for smooth manipulation and structural obstacle avoidance. In: 2014 IEEE International Conference on Robotics and Automation (ICRA), pp. 5127–5132 (2014)
28. Kamdar, S.: Design and manufacturing of a mecanum sheel for the magnetic climbing robot. Master Thesis, Embry-Riddle Aeronautical University (2015)
29. Ward, P., Manamperi, P., Brooks, P.R., Mann, P., Kaluarachchi, W., Matkovic, L., Paul, G., Yang, C.H., Quin, P., Pagano, D., Liu, D., Waldron, K., Dissanayake, G.: Climbing robot for steel bridge inspection: Design challenges. In: Austroads Publications Online, ARRB Group (2015)
30. Pham, N.H., La, H.M.: Design and implementation of an autonomous robot for steel bridge inspection. In: 54th Allerton Conf. on Comm., Con., and Comp., pp. 556–562 (2016)
31. Wang, R., Kawamura, Y.: Development of climbing robot for steel bridge inspection. Indust. Robot: Int. J. **43**(4), 429–447 (2016)
32. Pham, N.H., La, H.M., Ha, Q.P., Dang, S.N., Vo, A.H., Dinh, Q.H.: Visual and 3d mapping for steel bridge inspection using a climbing robot. In: The 33rd Intern. Symposium on Automation and Robotics in Construction and Mining (ISARC), pp. 1–8 (2016)
33. Takada, Y., Ito, S., Imajo, N.: Development of a bridge inspection robot capable of traveling on splicing parts. Inventions **2** (2017)
34. Versatrax: Versatrax 150^{TM}. http://inuktun.com/en/products/ (2019)
35. Sato, G., Mae, Y., Kojima, M., Arai, T.: Transfer motion on planar structure of limb-mechanism robot in anti-gravity environment. In: Proceedings of 2018 ISFA International Symposium on Flexible Automation, pp. 467–472 (2018)
36. Van Nguyen, L., Gibb, S., Pham, H.X., La, H.M.: A mobile robot for automated civil infrastructure inspection and evaluation. In: 2018 IEEE International Symposium on Safety, Security, and Rescue Robotics (SSRR), pp. 1–6 (2018)
37. La, H.M., Gucunski, N., Dana, K., Kee, S.-H.: Development of an autonomous bridge deck inspection robotic system. J. Field Robot. **34**(8), 1489–1504 (2017)
38. Gibb, S., Le, T., La, H.M., Schmid, R., Berendsen, T.: A multi-functional inspection robot for civil infrastructure evaluation and maintenance. In: 2017 IEEE/RSJ International Conference on Intelligent Robots and Systems (IROS), pp. 2672–2677 (2017)
39. Le, T., Gibb, S., Pham, N., La, H.M., Falk, L., Berendsen, T.: Autonomous robotic system using non-destructive evaluation methods for bridge deck inspection. In: 2017 IEEE International Conference on Robotics and Automation (ICRA), pp. 3672–3677 (2017)
40. La, H.M., Lim, R.S., Basily, B.B., Gucunski, N., Yi, J., Maher, A., Romero, F.A., Parvardeh, H.: Mechatronic systems design for an autonomous robotic system for high-efficiency bridge deck inspection and evaluation. IEEE/ASME Trans. Mechatronics **18**(6), 1655–1664 (2013)
41. La, H.M., Gucunski, N., Kee, S.-H., Nguyen, L.V.: Data analysis and visualization for the bridge deck inspection and evaluation robotic system. Vis. Eng. **3**(1), 1–16 (2015)
42. La, H.M., Gucunski, N., Kee, S.H., Nguyen, L.V.: Visual and acoustic data analysis for the bridge deck inspection robotic system. In: The 31st International Symposium on Automation and Robotics in Construction and Mining (ISARC), pp. 50–57 (2014)
43. Lim, R.S., La, H.M., Shan, Z., Sheng, W.: Developing a crack inspection robot for bridge maintenance. In: 2011 IEEE Intern. Conf. on Robotics and Automation (ICRA), pp. 6288–6293 (2011)
44. Lim, R.S., La, H.M., Sheng, W.: A robotic crack inspection and mapping system for bridge deck maintenance. IEEE Trans. Autom. Sci. Eng. **11**(2), 367–378 (2014)
45. Gibb, S., La, H.M., Le, T., Nguyen, L., Schmid, R., Pham, H.: Nondestructive evaluation sensor fusion with autonomous robotic system for civil infrastructure inspection. J. Field Robot. **0**(0) (2018)

46. Sutter, B., Lelevé, A., Pham, M.T., Gouin, O., Jupille, N., Kuhn, M., Lulé, P., Michaud, P., Rémy, P.: A semi-autonomous mobile robot for bridge inspection. Autom. Constr. **91**, 111–119 (2018)
47. La, H.M., Gucunski, N., Kee, S.-H., Yi, J., Senlet, T., Nguyen, L.: Autonomous robotic system for bridge deck data collection and analysis. In: 2014 IEEE/RSJ International Conference on Intelligent Robots and Systems, pp. 1950–1955 (2014)
48. Gillins, D.T., Parrish, C., Gillins, M.N., Simpson, C.: Eyes in the sky: Bridge inspections with unmanned aerial vehicles. https://www.oregon.gov/ODOT/Programs/ResearchDocuments/SPR787_Eyes_in_the_Sky.pdf (2018)
49. Eschmann, C.W., Kuo, C.-M., Kuo, C., Boller, C.: Unmanned aircraft systems for remote building inspection and monitoring. In: The 6th European Workshop on Structural Health Monitoring (2012)
50. Hallermann, N., Morgenthal, G.: Visual inspection strategies for large bridges using unmanned aerial vehicles (uav). In: Bridge maintenance, safety, management and life extension, pp. 661–667 (2014)
51. Zink, J., Lovelace, B.: Unmanned aerial vehicle bridge inspection demonstration project final report. http://www.dot.state.mn.us/research/TS/2015/201540.pdf (2015)
52. Dorafshan, S., Maguire, M.J.: Bridge inspection: human performance, unmanned aerial systems and automation. Civil Struct Health Monit (2018) (2018)
53. Intel-Drone. Intel Flies Drones for Bridge Inspection, December 07, 2018. Available at https://www.engineering.com/BIM/ArticleID/18113/Intel-Flies-Drones-for-Bridge-Inspection.aspx (2018)
54. K&J Magnetics, I.: Original magnet calculator. https://www.kjmagnetics.com/ (2019)

Son Thanh Nguyen (IEEE M'2019) received his B.S. degree in Mechatronic Engineering from Military Technical Academy, Hanoi, Vietnam in 2011, and M.S. degree in Control Engineering and Automation from Ho Chi Minh University of Transport, Ho Chi Minh City, Vietnam in 2015. He is currently working toward his PhD degree at the Advanced Robotics and Automation (ARA) Laboratory, Department of Computer Science and Engineering, University of Nevada, Reno, NV89557, USA. His research interest includes robotic design, robotic control, and automated civil infrastructure inspection.

Hung Manh La (IEEE M'2009, ASCE M'2020) received his B.S. and M.S. degrees in Electrical Engineering from Thai Nguyen University of Technology, Thai Nguyen, Vietnam, in 2001 and 2003, respectively, and his Ph.D. degree in Electrical and Computer Engineering from Oklahoma State University, Stillwater, OK, USA, in 2011. Dr. La is the Director of the Advanced Robotics and Automation (ARA) Lab, and Associate Professor of the Department of Computer Science and Engineering, University of Nevada, Reno, NV, USA. From 2011 to 2014, he was a Post Doctoral research fellow and then a Research Faculty Member at the Center for Advanced Infrastructure and Transportation, Rutgers University, Piscataway, NJ, USA. He has authored over 120 papers published in major journals, book chapters and international conference proceedings. His current research interests include robotic systems and mobile sensor networks. Dr. La is the recipient of the 2019 NSF CAREER award, and the 2014 ASCE Charles Pankow Award for the Robotics Assisted Bridge Inspection Tool (RABIT), eight best paper awards/finalists, and a best presentation award in international conferences (e.g., ICRA, IROS, ACC). Dr. La is currently an Associate Editor of the International Conference on Robotics and Automation (ICRA), the IEEE Transactions on Human-Machine Systems, the Journal of Drones, the Frontiers in Robotics & AI, and the International Journal of Robotic Engineering, respectively. Dr. La has served as an Associate Editor of the International Journal of Automation and Control, and a Guest Editor for International Journal of Robust and Nonlinear Control.